Engineering Reports

WILEY

Engineering Reports Open Access

RESEARCH ARTICLE OPEN ACCESS

Impact of Carbon Fiber-Reinforced Polymer Sheets and Bolt Diameter on the Seismic Performance Enhancement of Steel Beam-Column Joints

Fayiz Amin[1] | Hafiz Ahmed Waqas[1] | Ijaz Ali[1] | Muhammad Waseem[1] | Muhammad Asif[2] | Khan Abdul Majid[2] | Megersa Kebede Leta[3]

[1]Department of Civil Engineering, Ghulam Ishaq Khan Institute of Engineering Sciences and Technology, Swabi, Pakistan | [2]School of Architecture Engineering, Xi'an University of Technology, Shaanxi, China | [3]Faculty of Civil and Environmental Engineering, Jimma Institute of Technology, Jimma University, Jimma, Ethiopia

Correspondence: Megersa Kebede Leta (megersa.leta@ju.edu.et)

Received: 19 June 2024 | **Revised:** 22 September 2024 | **Accepted:** 26 September 2024

Funding: The authors received no specific funding for this work.

Keywords: CFRP | extended end plate | finite element analysis | prefabricated steel connection | seismic performance

ABSTRACT

Beam-column joints are pivotal for ensuring the resilience of prefabricated steel structures under various loading conditions. Following the major earthquakes of the 1990s, semi-rigid bolted connections emerged as a promising alternative to traditional welded connections. This study investigates a fully prefabricated Intermediate Beam-Column Joint (IBCJ) with extended endplates, renowned for its excellent seismic resistance. While significant progress has been made in existing research, there is still a need to thoroughly examine the tension capacity of IBCJs concerning bolt size and explore the potential of Carbon Fiber-Reinforced Polymer (CFRP) sheets to enhance joint performance under seismic loading. Using the finite element method, this research evaluates the performance of IBCJ under both monotonic and cyclic loading conditions. After validation with experimental data, the study examines various bolt diameters to assess their tension capacity, ductility ratio, secant stiffness, and energy dissipation capacity. The findings indicate that larger bolts exhibit higher ultimate capacities and reduced deformation at failure. Additionally, the study investigates the optimal placement and configuration of CFRP sheets, identifying the backside of the endplates as the most effective location. The application of CFRP significantly enhances bolt tension capacity by up to 1.2 to 1.3 times, demonstrating its potential in reducing bolt failure risk and improving structural reliability under seismic conditions. The superior performance of CFRP-strengthened bolts can play a crucial role in the design and retrofitting of prefabricated steel structures, potentially contributing to the improvement of existing standards and practices of seismic enhancement of IBCJ.

1 | Introduction

Prefabricated steel structures, referred to as offsite construction, or industrialized or modular housing, have emerged as a favored solution in rapidly growing cities, addressing population booms and labor shortages [1]. This construction method significantly reduces time by allowing simultaneous development of structural elements [2]. Over the past century, prefabrication has gained traction for its reliability and cost-effectiveness amidst growing concerns about environmental and economic impacts of traditional construction [3]. Developed nations like the UK, US, and China have embraced prefabrication to enhance construction

efficiency, with materials like steel proving ideal due to their strength, lightweight nature, and machinability [4–6]. Prefabrication, aligning with green construction principles, addresses waste management and environmental concerns but faces challenges like unit scarcity and construction layout limitations [6].

The essence of Prefabrication lies in the ductility, stiffness, and strength of beam-column joints which are crucial for steel structure design [5]. Recent seismic events like the 1994 Northridge earthquake, the 1995 Hanshin earthquake [7, 8], and the 2015 Nepal earthquake [6] highlighted concerns over the stability and seismic performance of these connections in terms of severe brittle failure [9]. Despite their importance, steel structure connections haven't received ample attention, with weak links often overlooked [10, 11]. There's a pressing need for designers and engineers to understand these connections profoundly. Designing steel connections demands the integration of theoretical, experimental, and contemporary computer simulation methods to ensure durability, structural strength, and sustainability of steel structures. Standardized procedures guide connection design globally, emphasizing factors such as force distribution, strength, ductility, corrosion protection, weld fracture susceptibility, fatigue resistance, serviceability requirements, and seismic performance [12].

Connections are categorized as fixed or pinned, each exhibiting different rotational capabilities and practical behaviors. Semi-rigid connections have gained attention for their reliable designs and economic benefits, particularly in seismic areas [13]. They offer ductility, controlled rotation, and partial strength, all essential for minimizing deflection [14]. While nonlinear tendencies such as material discontinuities, stress concentration, local yield, connection buckling, and geometric changes under load pose challenges in modeling, understanding their behavior is imperative. These tendencies may worsen in bolted semi-rigid connections such as endplate and T-subs connections, due to diverse connection configurations, stress concentrations, and frictional and prying forces [15]. Hence, their understanding and design has progressed mainly through Finite Element Analysis (FEA) [13].

Extensive studies have examined end-plate-bolted connections, considering factors like end-plate thickness, stiffener type, beam/column dimensions, and steel yield strength to enhance ductility and seismic resistance [16, 17]. Investigations on varied end-plate thicknesses and bolt diameters have shown their impact on beam-column joint response, highlighting the importance of exploring bolted connections further to improve the overall structural performance [13]. While welded connections were initially prevalent, the drawbacks of its rigid behavior such as susceptibility to brittle failure due to residual stresses, and challenges in repair and maintenance prompted a quest for alternatives [18]. Post-earthquake experimental investigations exposed these drawbacks, leading to the prominence of bolted connections [8]. Studies have recognized the semi-rigid behavior of endplate bolted connections under cyclic and monotonic loading conditions [19].

Luo et al. [18] assessed the seismic performance of extended end-plate connections subjected to cyclic loads, confirming their semi-rigid behavior and the agreement between experiment and FEA. Chung et al. [19] analyzed the structural behavior of bolted connections in cold-formed steel using FEA. They revealed failure patterns such as net section failure, shear-out failure, and bearing strength failure, thus demonstrating the reliability of analytical approach. Maggi et al. [13] used FEA to study end-plate connections, confirming relevant failure mechanisms and considering factors like end-plate displacement, connection stiffness, and bolt forces.

Mashaly et al. [20] utilized a novel shell bolt approach to model bolts. FEA results aligned closely with experimental results, yet cyclic loads demanded more streamlined FEA for efficiency. Similarly, Ali et al. [21] developed a Finite Element Modeling (FEM) approach for predicting structural behavior in cold-formed steel connections. They employed section elements for structural components and bar elements to simulate bolt fastening, which proved efficient in predicting structural behavior. Liu et al. [5] highlighted the favorable traits of bolted-welded connections, that is, good energy dissipation, ductility, rotation capacity, and seismic resilience through cyclic and monotonic load testing, with plastic rotation angles meeting seismic criteria. Expanding their expertise, they introduced an innovative steel connection type for high-rise construction, showing column stiffness adjustment by varying the number of bolts [22].

The type, strength, number, size, or tightening of bolts play a crucial role in the response of beam–column joints to various loading. Ismail et al. [23] developed a comprehensive FEM approach to analyze end-plate steel connections under monotonic loading, assessing various bolt parameters' impact on connection behavior. In flush type connections, increasing bolt diameter from 20 to 24 mm can significantly enhance ultimate moment by 14% and rotation capacity by 63% and further increase to 27 mm results in a 3.5% improvement in both. Rib stiffeners in extended end plates further boost initial stiffness by 60%–90% and ultimate moment by 140%. Dessouki et al. [24] contributed by proposing design equations for extended end-plate moment connections, validated through rigorous comparisons with FEA results and existing design standards. These findings highlight the importance of optimizing bolt selection and end-plate design for stronger and more efficient bolted connections.

The experimental studies of Chen et al. [25] revealed that larger bolt diameters enhance load-carrying capacity and stiffness of joints. Fan et al. [26] investigated the junction between a double-skin steel tubular (CFDST) column filled with concrete and a steel beam, finding that increased endplate thickness significantly improved seismic performance, while axial compression ratio, bolt diameter, and inner tube shape had specific impacts on mechanical response [26]. ElSabbagh et al. [27] explored extended endplate bolted connections' response to cyclic and monotonic loadings, emphasizing shear force's influence on connection stiffness [27].

New techniques for strengthening steel and concrete structures include Fiber Reinforced Polymers (FRP). Among them, Carbon Fiber-Reinforced Polymer (CFRP) is a composite material made of carbon fibers embedded generally in an epoxy resin matrix. The fibers result in a higher tensile strength while the polymer matrix offers flexibility [28]. Its advantages include a high strength-to-weight ratio, comparable to steel, enhanced resistance to corrosion and fatigue, and customizable properties

like fiber type, orientation, and volume fraction [29]. It is extensively used for strengthening and repairing existing structures, particularly in seismic retrofitting, offering enhanced strength, ductility, and energy dissipation [29, 30]. CFRP laminates and strips are widely recognized as one of the most effective methods for strengthening various reinforced and prestressed concrete elements such as by [31]. However, their application in steel structures remains limited [31]. Researchers like Miller et al. [32], Liu et al. [33], Cadei et al. [34], and Syed-Ahmed [35, 36] have applied CFRP to the tension flanges of beams to enhance their flexural strength. Ghareeb et al. [37] focused on increasing the flexural strength of I-section steel beams by applying CFRP laminates to their webs. Shekarchi et al. [38] explored the shear and flexural performance of structural steel beams reinforced with high-modulus CFRP laminates, noting significant improvements in yield load, ultimate load capacity, and energy absorption. Colombi et al. [39] used CFRP strips to reinforce bolted joints, examining local stresses near lamina edges and discontinuities (like holes) and assessing the bearing capacity of the CFRP strips.

Despite significant research on Intermediate Beam-Column Joints (IBCJs) with extended end plates, there exist notable gaps. While all these studies have investigated the impact of different physical parameters on beam-column joint capacity, fewer have explored the increasing trend of joint ductility with increasing bolt diameter such as by [18, 40]. This study steps further to determine the performance of bolt diameter for IBCJs with extended endplates, specifically subjected to cyclic loads and in the light of various seismic parameters such as joint and member tension capacity, energy dissipation, stiffness degradation, and ductility ratio under both cyclic and monotonic loading conditions. Prior to this, a representative numerical model of a beam-column joint was created and calibrated based on experimental data to ensure accuracy. Five beam-column joint configurations, each featuring different bolt sizes, were modeled and analyzed for bolt tension capacity under cyclic and monotonic loading. The load carrying capacity skeleton curves, cumulative energy dissipation, secant stiffness and ductility ratio were analyzed for performance assessment of these joints.

Moreover, for the behavior of CFRP strengthened beam-to-column joints, design guidelines are currently very limited [19]. Most previous studies have focused on the moment-rotation behavior of these joints under monotonic loading conditions [41–48]. Few studies have addressed the cyclic performance of FRP strengthened beam-column joints, but they primarily concentrate on the development of connection components such as cuffs, sleeves, or universal connectors, rather than directly examining the cyclic behavior of the joints themselves [49–55]. Like Smith et al. [49] found that innovative connection details for GFRP box section beams and columns significantly enhanced joint stiffness and strength, with observed increases of 90% and 330%, respectively, compared to standard steel-based designs. A study by Moghadam et al. [56] analyzed the application of CFRP in retrofitting steel elements where they found that using CFRP with a higher elastic modulus and appropriate adhesives significantly enhances bond strength, structural load-carrying capacity, flexural strength, and fatigue life of retrofitted steel components. Accord et al. [57] also used FEA to evaluate how the placement of GFRP strips affects the ductility of cantilever I-section beams. They found that positioning the GFRP strips away from the web-flange junction leads to enhanced ductility in the members. However, on the other hand, Ragheb et al. [58, 59] found that positioning CFRP strips near the web-flange junction significantly enhances the ultimate load capacity. Liu et al. [60] investigated the effectiveness of CFRP sheets in enhancing the fatigue life of steel plates, revealing that double-sided repairs significantly outperformed single-sided repairs, with high modulus CFRP sheets increasing fatigue life by up to 7.9 times. However, this study has independently studied the steel plates and not in context of steel beam-column joints.

Hence, although the impact of CFRP on the flexural or shear capacity of beam or columns or independently the steel plates has been studied [61], the potential of using CFRP sheets in the beam-column joint, particularly on the endplates to improve the joint tension capacity has not been thoroughly explored. Therefore, this numerical study aims to investigate the effectiveness of CFRP sheets in enhancing joint capacity and assessing its practical feasibility to the endplates under both cyclic and monotonic loading. Through parametric study, this study also aims to determine the most suitable position of CFRP sheets to apply at the beam-column joint. Furthermore, the determined optimum application of CFRP sheet is utilized to investigate the joint capacity with different bolt sizes under cyclic and monotonic loading complemented by CFRP sheets.

In a nutshell, this study addresses critical gaps in the understanding of IBCJs with extended end plates, focusing on the impact of bolt diameter on joint performance under cyclic and monotonic loadings, and the potential application of CFRP sheets to enhance joint capacity. The research aims to optimize bolt selection and explore innovative CFRP applications for improving seismic resilience in steel structures. The findings can significantly advance sustainable structural engineering practices, enhance the safety and longevity of steel structures in seismic regions, and contribute to more resilient urban infrastructure. The overall methodological framework is presented in Figure 1.

2 | Materials and Methods

FE modeling and analysis has emerged as a more efficient alternative to traditional laboratory testing. It offers a streamlined approach to structural analysis by breaking down complex structures into smaller meshed components. This approach has gained attention from structural analysts worldwide for its efficiency [16]. Abaqus/CAE, used in this study, is a reliable FEM tool and is widely utilized for modeling and analyzing steel beam column joints [20], [56–58].

2.1 | Model Description

The model comprises steel beams, steel columns, end plates, high-strength bolts, and other components. It is constructed in Abaqus using geometric details from the experimental tests conducted by Luo et al. [18]. To align with the study objectives, every section in the end-plate connection joint is carefully designed according to established steel structure design specifications, that

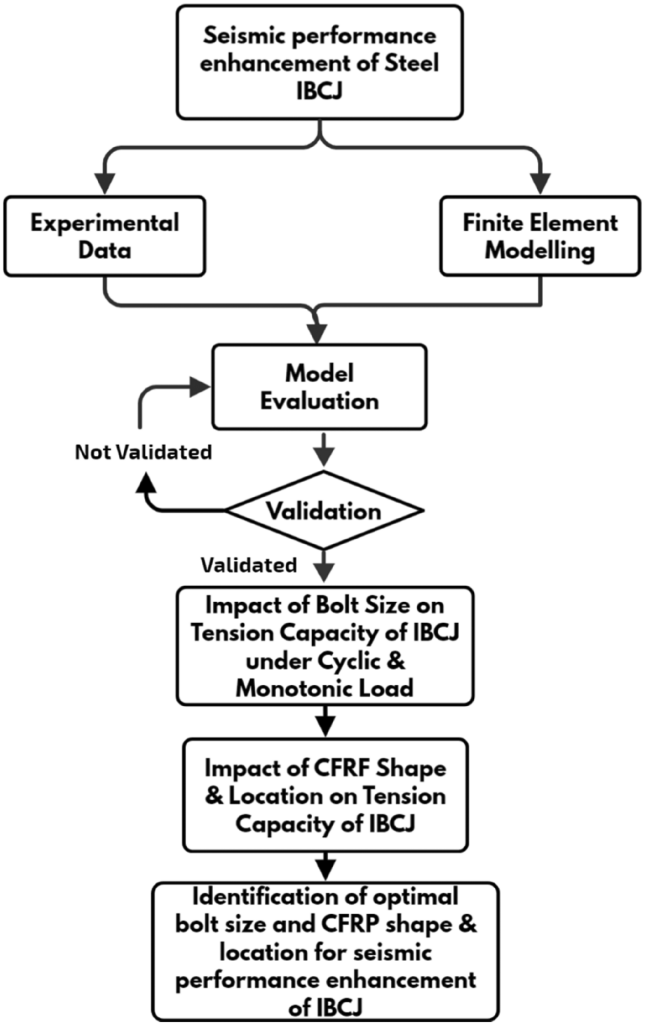

FIGURE 1 | Methodological framework of the present study.

is, Chinese National Standards (GB). The specimen arrangement involves an IBCJ with extended endplate bolted connections, utilizing variable parameters such as connection type, bolt size and end-plate thickness, summarized in Table 1. Before assembling, the connected components were sandblasted to achieve a friction coefficient of 0.44 on the contact surface. To fasten the beam and column, friction-type high-strength bolts of 10.9-grade were utilized. The 10.9 grade M20 bolts were tightened initially to 280 N-m and finally to 446 N-m. A 2 mm gap was assured between the bolt and the bolt hole. The joint's fundamental configuration, depicted in Figure 2, features beam and column dimensions, with a steel strength grade of Q345B as per GB-50017-03 [62, 63]. Detailed properties of Q345B steel are given in.

Table 2. The endplate is connected to the beam through fully penetrating butt welds utilizing E50 welding rods. Additionally, material property tests conducted, following GB/T228.1-2010 regulations, are summarized in Table 2 [64, 65].

The height and width of endplate (h_{ep} and b_{ep}) are calculated based on the beam and column dimensions according to $h_{ep} = h_b + 2\ (e_f + c)$, $b_{ep} = t_{bw} + 2\ (e_s + e_w)$ and $b_{bf} \le b_{ep} \le b_{cf}$. As shown in Figure 2a, h_b represents the height of beam, e_f is the

TABLE 1 | Geometric details of the sample.

Sample	Dimension (mm)
Stiffener	12
Beam web	8
End-plate	16
Column flange	15
Column web	10
Beam flange	12
M20 bolt	20

distance from the outer edge of the beam flange surface to the top row of bolts, c indicates the distance from the outer border of the endplate to the top row of bolts, b_{bf} is the beam flange width, and b_{cf} denotes the column flange width. The end-plate thickness, as per the GB-50017-03 guidelines, should be 12 mm or more, typically ranging from 12 to 25 mm [62]. For this study, a thickness of 16 mm has been opted.

The bolt configuration also follows GB-50017-03 guidelines which suggest a symmetrical arrangement of bolts, preferably in two columns, for the end-plate connection. According to the codes [62], the column web thickness (t_{cw}) must meet stability criteria [$t_{cw} \ge (h_{bw} + h_{cw})/90$], with flanges locally thickened for stability during the test, except for edge column joints. Here, as depicted in Figure 2b, h_{bw} represents the height of the beam web and h_{cw} indicates the height of the column web. Stiffeners of the column web comply with specific criteria [$t_s \ge t_{bf}$, $h_s = h_c - 2t_{cf}$, $b_s = 0.5\ (b_{cf} - t_{cw})$], t_s indicates the thickness of the column web stiffeners, t_{bf} and t_{cf} represent the thickness of the beam and the column flange, h_s and b_s depict the column web stiffener's height and breadth and h_c and b_c stand for column section height and width, respectively. Figure 2c illustrates the sectional detailing of the beam and column, while Figure 2d displays the end plate joint specifications used in FEM. The entire beam-column joint assembly, shown in both 3D and 2D, is depicted in Figure 3a,b.

2.2 | Modeling of Steel Materials

The numerical model simulates the mechanical response of the joint specimen by utilizing a multi-linear steel stress–strain correlation. A bilinear kinematic hardening model, suitable for high-strength steel, is employed as the constitutive model of the high-strength bolt to account for its plastic hardening behavior. To replicate the real-world behavior of steel and bolt, elastic–plastic modeling technique is utilized as illustrated in Figure 4a,b.

Table 2 provides a detailed description of the mechanical characteristics of bolts and structural steel materials.

2.3 | Modeling of CFRP

In this study, the lamina elastic model and Hashin damage mechanism were chosen, with a thickness of CFRP sheets as 0.25 mm.

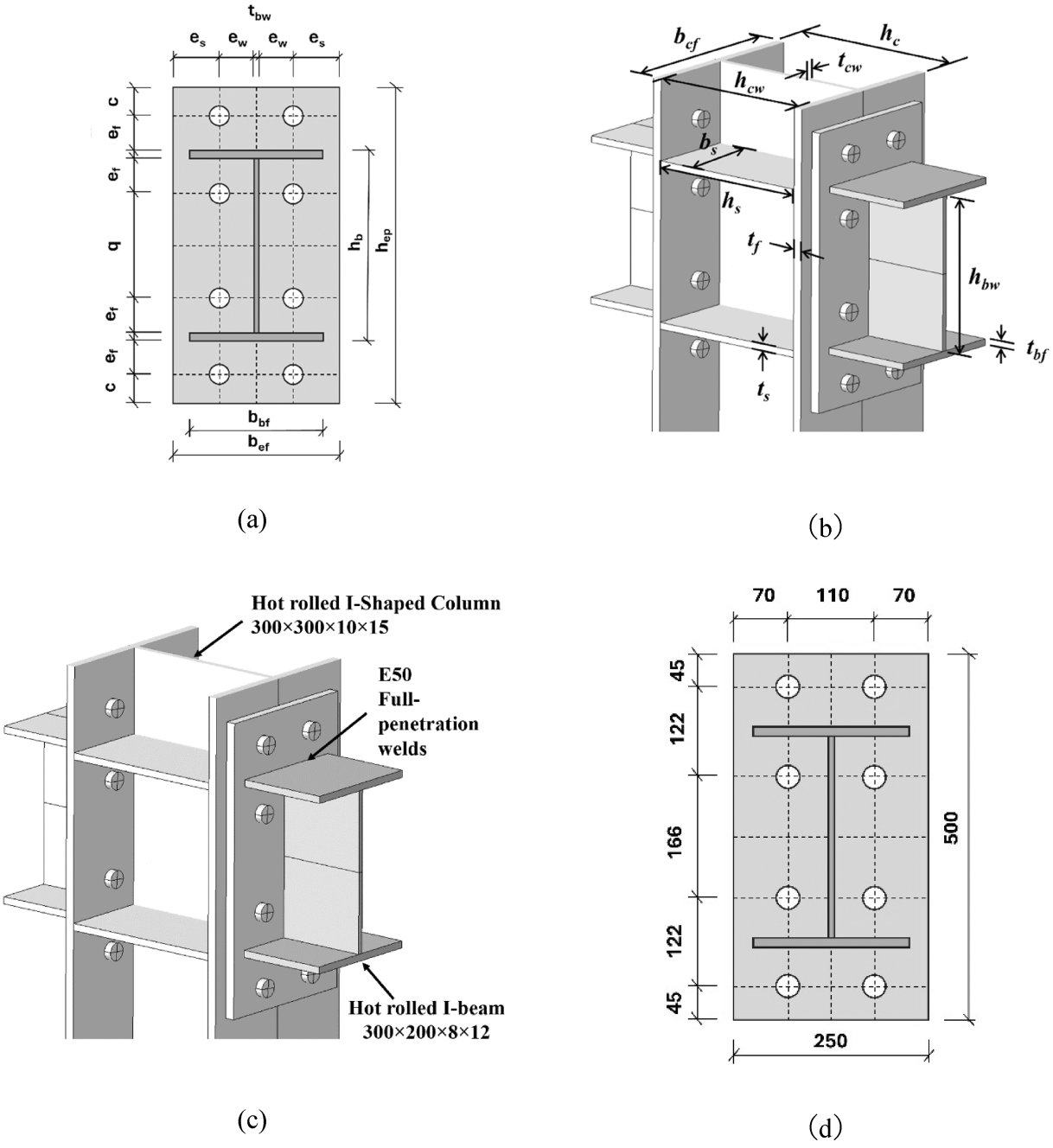

FIGURE 2 | Design details: (a) End-plate connection parameters, (b) Joint parameters, (c) Sectional detailing of the beam and column, and (d) End plate joint specifications (mm).

TABLE 2 | Material properties of steel and bolt.

Type of Material	E (GPa)	f_y (MPa)	f_u (MPa)	Density (kg/m^3)
Q345B steel	207.27	370.16	556.2	7850
10.9-grade high strength bolt	208.23	987.55	1182.1	7850

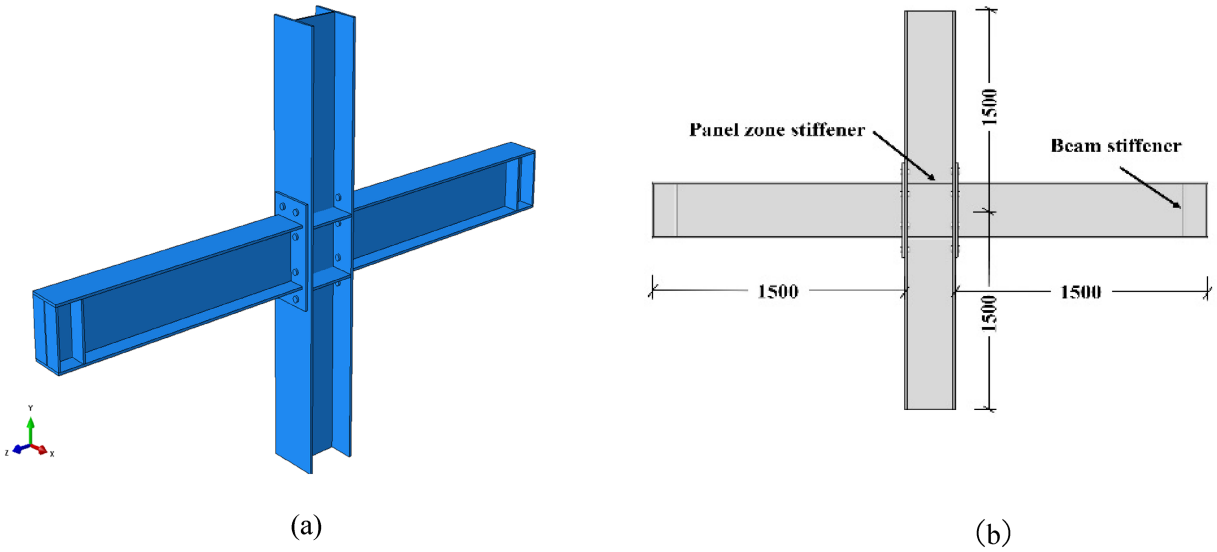

FIGURE 3 | Model Assembly: (a) 3-D representation and (b) IBCJ dimensions.

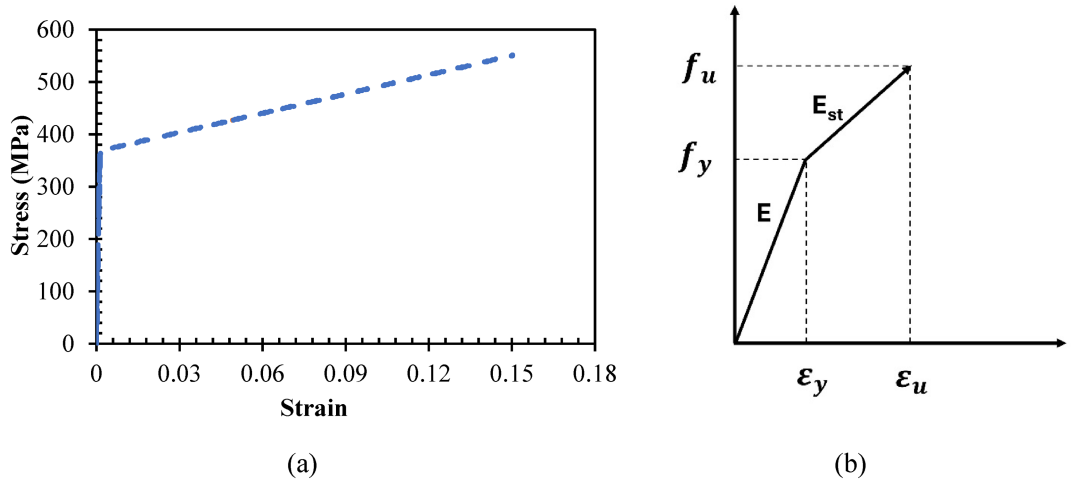

FIGURE 4 | Constitutive models for (a) Steel and (b) Bolt.

Hashin cracking, titled after extensive work on damage behavior of composites by Hashin, represents a propagating crack [66, 67]. It is ideal for modeling and simulating the damage behavior of CFRP. The CFRP material was applied at the respective endplates of IBCJs with different variations. The location of its application is described in upcoming Section 3.8 and depicted in Figure 15. The material properties for modeling the CFRP, sourced from existing literature [62, 68, 69], are detailed in Tables 3–5.

2.4 | Interactions, Boundary Conditions, and Load Scheme

The experimental setup has employed an MTS hydraulic servo loading system. The setup included essential elements such as beams, columns, connections, MTS actuators, loading jacks, and lateral and hinged supports. As shown in Figure 5, the column's top was secured to a sliding support through a ground anchor, its bottom was fixed to a hinged base and the beam tips were hinged. Seismic loads were applied utilizing a hydraulic servo actuator, following the loading procedure established by the SAC Joint Venture (1997) [70].

In the numerical modeling scheme, specific components of the IBCJ hold significant potential for contact. These interactions include the bolt with the plate, column flange, beam flange, and end-plate surface; the steel connection plate with the steel beam flange; the stiffeners with the beam and column; and the steel column flanges with the end plate. To define these interactions, the stiffer surface is designated as the master surface, while the other is the slave surface. The screw/bolt surface serves as the master surface in its interaction with the steel beam and column flanges, which are defined as the slave surfaces.

Coupling interaction is defined on the column's top side with its surface to prepare it for cyclic loading. A tie constraint contact is applied, neglecting the residual deformation and stress concentration caused by the high-temperature welding of the peripheral plate. Tie contact is employed to represent the welding connection of the steel beam and endplates. For surface interaction

TABLE 3 | Elastic properties of CFRP.

Density (kg/m^3)	E1 (MPa)	E2 (MPa)	Nu12	G12 (MPa)	G13 (MPa)	G23 (MPa)
1560	130,000	8000	0.28	4500	4500	3600

TABLE 4 | Hashin damage definition for CFRP.

Longitudinal tensile strength (MPa)	Longitudinal compression strength (MPa)	Transverse tensile strength (MPa)	Transverse compression strength (MPa)	Longitudinal shear strength (MPa)	Transverse shear strength (MPa)
2200	2200	61	130	85	40

TABLE 5 | Hashin damage evolution for CFRP.

Longitudinal tensile fraction energy (mJ/mm^2)	Longitudinal compression fraction energy (mJ/mm^2)	Transverse tensile fraction energy (mJ/mm^2)	Transverse compression fraction energy (mJ/mm^2)
70	70	0.25	0.25

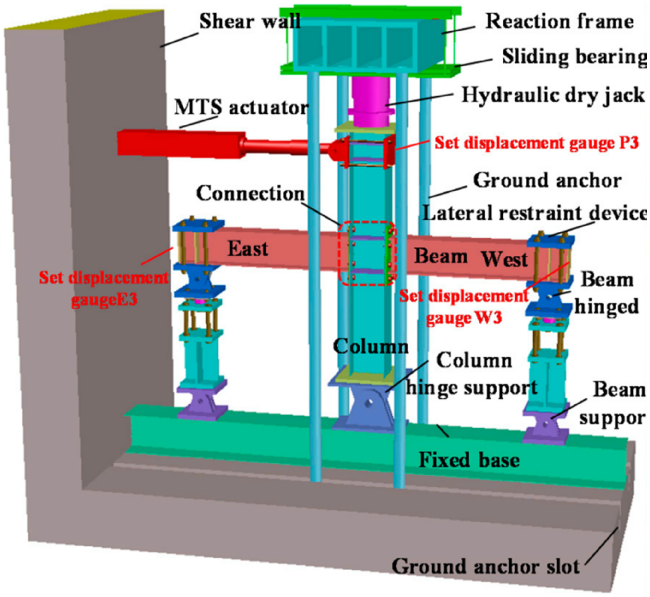

FIGURE 5 | Schematic representation of experimental setup [18].

among other components, a tangential penalty function and normal hard contact are utilized. For normal contact, hard contact replicates the extrusion case of the bolt and plate. For tangential contact, a penalty function models friction, with a coefficient of 0.44 between the flange of the column and the endplate.

Boundary conditions and loadings were carefully applied to replicate the experimental setup in the FEM, ensuring efficiency and accuracy. Both ends of the beam were assumed pinned, while the column bottom was treated as fixed. Moreover, for the high-strength bolt's pretension force, a 10 N force for bolt pre-tightening was initially applied followed by a full 155 kN pretension force. As a whole, each analysis underwent three types of loadings: a constant load on the center of bolt shank for pretension force, an axial load of 600 kN on top of the column, and an incremental cyclic load on the beam tip in the form of displacement to generate a bending moment on the connection. Figure 6a visually depicts the cyclic loading protocol for the numerical model in terms of displacement, while Figure 6b illustrates the application of loading and the delineation of boundary conditions within the numerical model.

2.5 | Meshing of the Numerical Model

In FEM, mesh quality and density are significant for its computational efficiency. Areas with notable stress gradient changes and stress concentration require careful meshing for accurate calculations. For the model under study, the Continuum 3-Dimensional, 8-node elements with Reduced integration (C3D8R) are chosen for meshing due to its compatibility with modeling complexities and efficiency in curtailing the expansion of the hourglass effect. This element type not only accelerates model calculations but also prevents shear locking phenomena to provide desirable results. Moreover, regarding the size, high-strength bolts are assigned dense meshes of 5 mm, stiffeners and extended plates with refined meshes of 50 mm, and beams and columns with comparatively sparse grids of 60 mm. Each mesh has been assigned optimally after carefully checking the model sensitivity to the mesh size, as discussed in the sensitivity analysis using various mesh trails in the model validation section. The meshed geometry of IBCJ, bolt and endplate are depicted in Figure 7.

3 | Results and Discussion

3.1 | Mesh Sensitivity Analysis

Mesh sensitivity analysis evaluates the impact of varying mesh sizes on the structural response, results accuracy, and computational efficiency. By systematically varying mesh sizes and comparing results, the study identified optimal mesh sizes that balanced computational efficiency with result accuracy. It investigated six sets of meshes for beam and column, bolts, and

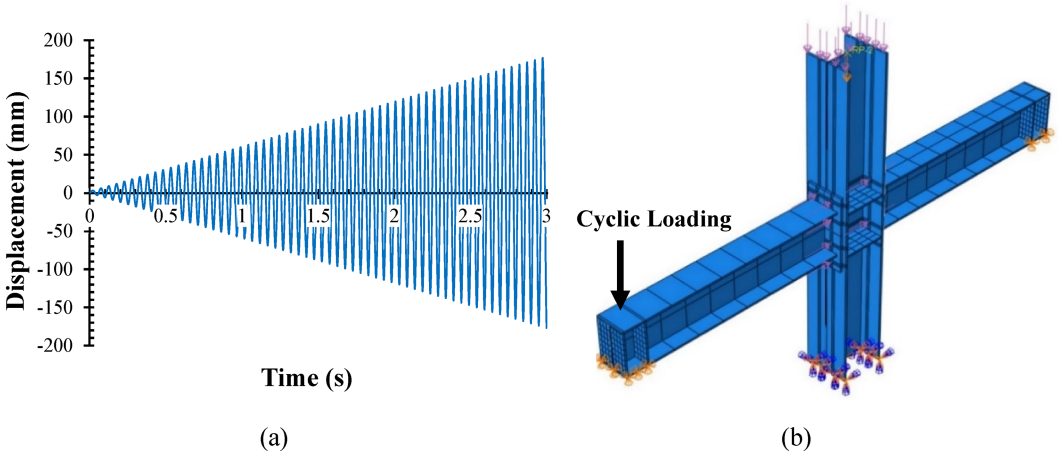

FIGURE 6 | Loading scheme in the FE model: (a) Introduced reverse cyclic loading and (b) Schematic representation of loading and boundary conditions.

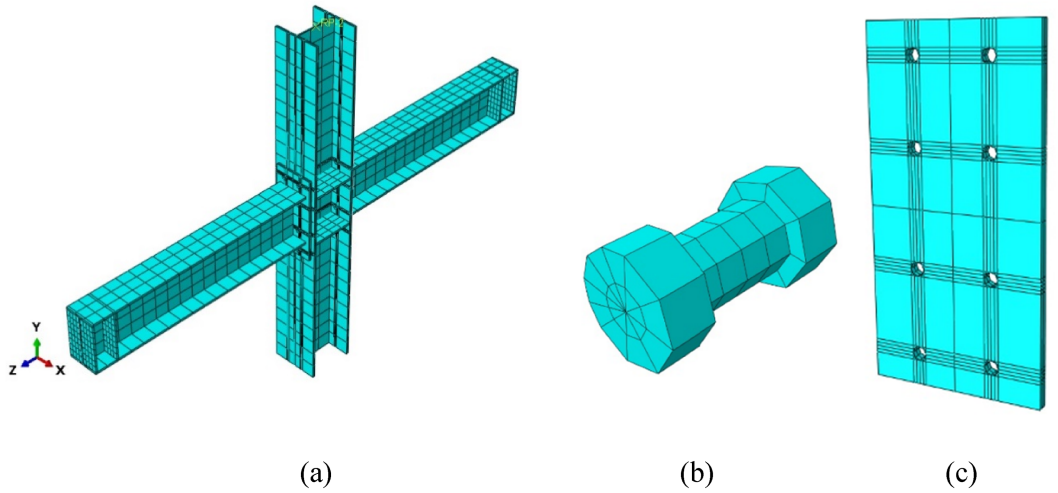

FIGURE 7 | Meshing (a) Whole assembly, (b) Bolt, and (c) Extended endplate.

plates as detailed in Table 6. The findings indicated that refining the mesh beyond 60 mm for beams and columns, 5 mm for bolts, and 50 mm for plates did not significantly alter the joint response. While smaller mesh sizes below 60 mm produced only minor changes, the outputs were not notably impacted due to the small element size. Therefore, a slightly larger element size was selected to reduce computational time. Figure 8 visually represents the impact of mesh size on modeling and simulation accuracy, reinforcing the validity of chosen mesh sizes and instilling confidence in the numerical analysis results.

TABLE 6 | Mesh sizes set for mesh sensitivity analysis.

	Mesh Size (mm)		
Mesh Name	**Beam and column**	**Bolts**	**Plates**
Mesh-1	100	8	70
Mesh-2	80	5	60
Mesh-3	60	5	50
Mesh-4	50	3	30
Mesh-5	40	2.5	25
Mesh-6	30	2	20

3.2 | Model Validation

In the model validation phase, a comparison between the FEM results and the outcomes of the experimental setup was conducted. The objective was to assess the FEM's capability in accurately predicting the behavior of IBCJ under earthquake loads. The outcome of experimental testing portrayed the failure patterns of joint that offer tangible evidence of the observed structural behavior. The beam flange buckling, tearing extending to the beam web, and significant bulging of the beam web was observed during the experiment. The comparison with the experimental results confirms the predictive capabilities of the FEM and helps understand the complex performance of various structural components of IBCJ.

Upon comparing, moment-rotation curve and peak-load from experimental results with numerical analysis exhibited close

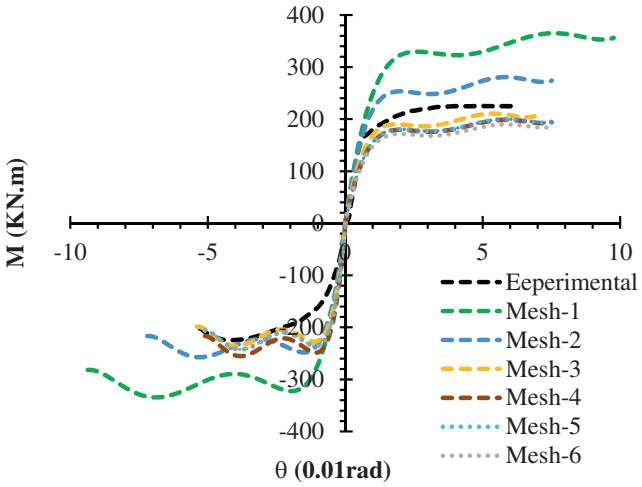

FIGURE 8 | Impact of mesh size on the accuracy of modeling results.

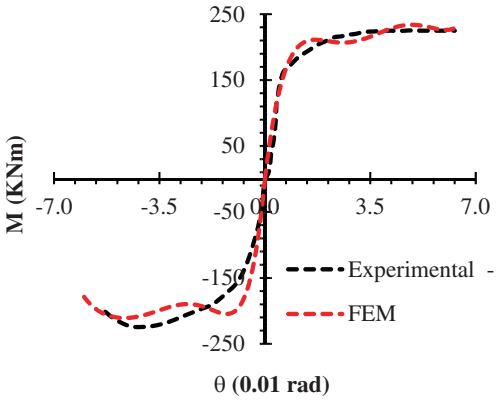

FIGURE 9 | Skeleton curves comparison—FE model versus experimental results of positive and negative sides of moment rotation curve.

TABLE 7 | Comparison of experimental and FEM results: Peak Moment (kN m).

Name	Experiment	FEM	Experiment/FEM
IBCJ	219.15	223.31	0.98

correspondence, as illustrated in Figure 9 and Table 7, respectively. Seismic response parameters such as load carrying capacity and skeleton curve were carefully compared with experimental outcomes. The skeleton curves derived from cyclic analysis showcased near-identical behavior in the elastic phase, gradually diverging as the connection yielded, however maintaining a consistent overall trend.

Shown in Figure 10, the numerical model accurately predicted a similar failure pattern in the IBCJ as observed during the test. When cyclic loading reached 130 mm displacement, equivalent to 0.06 rad, brittle failure occurred as illustrated in Figure 10a. This was due to sudden cracking of the weld between the endplate at the left side beam and lower flange of the beam. Simultaneously, the endplate detached from the column flange, with the upper two rows of bolts bearing the highest tension load, often leading to either breaking or necking. The sudden breakage of the upper bolts caused sharp unloading, resulting in bending of axes of bolts at the bottom two rows, as seen in Figure 10b. The maximum principal plastic strain, PE is provided in this figure to exhibit the damage distribution.

3.3 | Bolt Tension Response to Monotonic Load

After validating the model, an assessment was undertaken to identify the optimal bolt type capable of securely holding the connection during a seismic activity and in turn, to avoid brittle failure. Building upon the concepts of previous studies that indicate the crucial contribution of bolt size [8, 18, 40, 71], this study conducted a comprehensive analysis to assess the impact of varying bolt sizes on the IBCJ seismic performance. Five IBCJs with different bolt diameters, that is, 20 mm (D20), 24 mm (D24), 26 mm (D26), 30 mm (D30), and 35 mm (D35) were analyzed to identify the optimum bolt size. A mesh sensitivity analysis was performed to determine the model performance in comparison with the experimental results.

This type of analysis involved applying a monotonic displacement-controlled load of 150 mm on the beam tip, along with axial and bolt loading. The evaluation of tension capacities for various bolt diameters ranging from 20 to 35 mm provided detailed performance of extended end plate connection of the IBCJ. Results in Figure 11 indicated that for D20 and D24, increasing bolt diameter did not significantly enhance tension capacity. However, a slight improvement was observed in the D26 bolt. Moreover, larger diameters like D30 and D35 exhibited higher capacities which can be attributed to corresponding enlargements of bolt grip in the connection plate, allowance for greater engagement and distribution of load, and in turn enhanced tension capacity. However, further enlargement of holes beyond a certain point may result in diminishing returns. Hence, a careful balance between bolt diameter and hole size is essential for optimal performance.

Similarly, in a comprehensive comparison of yield and ultimate capacities of different bolt types, the most suitable bolt size for the connection was determined. The yield and ultimate capacities along with deformation observed at the failure point are presented in Table 8. It reveals that the D20 bolt exhibited more deformation at the point of failure and had a lower ultimate capacity compared to other bolts.

3.4 | Bolt Tension Response to Cyclic Load

For the cyclic load assessment, the cyclic load on the beam tip, along with the axial and bolt load, was applied. Analysis for the results of obtained tension capacity load versus displacement curves are presented in Figure 12, highlighting the impact of bolt diameter on tension capacity under cyclic loading. For instance, D20 bolt showed the lowest tension capacity (˜370 kN), while larger sizes (D24, D26, D30, and D35) exhibited higher capacities. The similar capacities observed for the D30 and D35 bolts can be attributed to the increased grip to the steel plate areas to better hold the beam and column together.

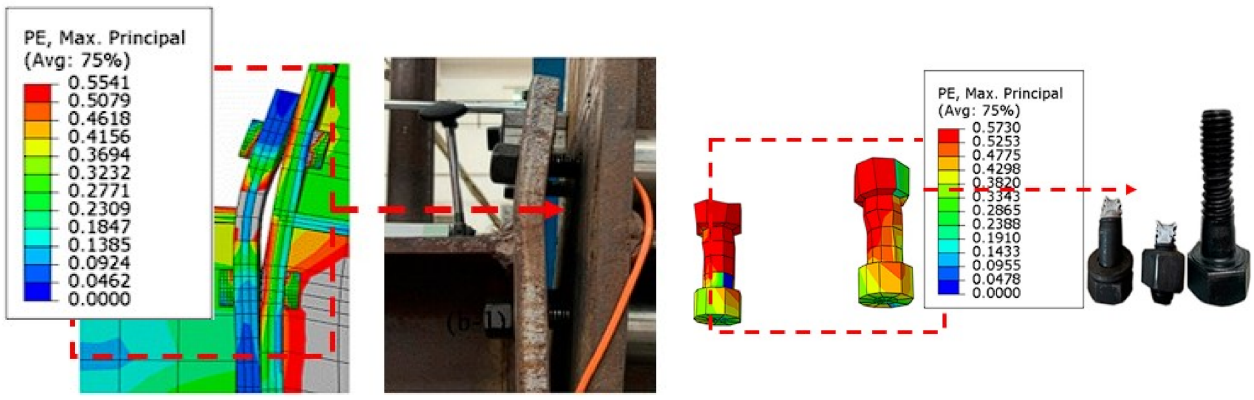

FIGURE 10 | Comparison of Failure modes between developed FE Model and experimental work of Luo et al. (a) Failure of end plate and (b) Failure of bolts.

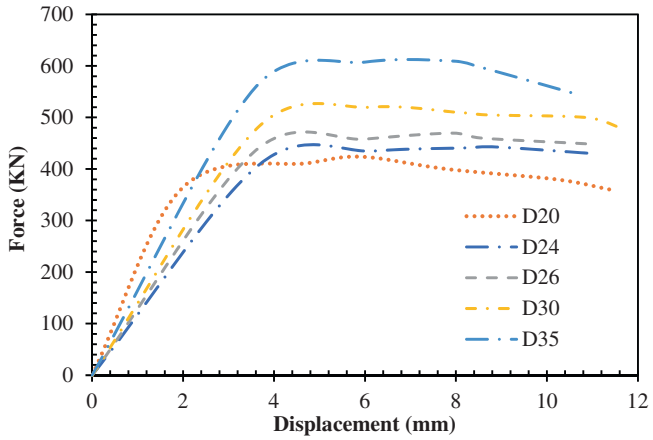

FIGURE 11 | Tension capacity across selected bolt sizes.

TABLE 8 | Comparison of ultimate load, yield load, and deformation at failure.

Bolt type	Yield load (kN)	Ultimate load (kN)	Deformation at peak (mm)
D20	557.6	423.8	3
D24	410	435	5
D26	434	458	4.3
D30	480	525	4.2
D35	557	610	5.6

3.5 | Ductility Ratio

Ductility plays a key role in seismic design considerations as it measures the structure's capability to absorb energy and deform plastically during earthquakes. The role of μ is central in modern seismic design approaches like Performance-Based Design (PBD) or capacity design [72]. In seismic zones, higher ductility ratios allow structures to absorb and scatter seismic energy effectively, thereby reducing the risk of abrupt failure [73]. This ratio is evaluated as below [74]:

$$\text{Ductility Ratio } (\mu) = \frac{\text{Deformation at Failure}}{\text{Deformation at Yield}} \quad (1)$$

Table 9 outlines the results regarding the ductility of bolted connections in IBCJs. The results indicate that the μ value decreases with larger bolt sizes. Bolts D20~D26 bolts exhibit almost similar μ values, suggesting comparable ductility levels. This allows for flexibility in bolt selection based on factors like availability, cost, or specific project needs. However, D30 and D35 bolts demonstrate comparatively smaller μ values, indicating lower ductility. Thus, prioritizing bolts size with a balance of strength and ductility requirement can enhance the seismic performance of connection, crucial for maintaining structural integrity under dynamic loading conditions.

3.6 | Secant Stiffness

During a seismic activity, structures experience significant deformations due to yielding, geometrical complexities and non-linear materials response. In this context, the secant stiffness dynamically adjusts to reflect the evolving stiffness throughout the deformation process and aids in predicting structural responses accurately [75]. The fluctuation in equivalent stiffness indicates the seismic performance, showing how joint stiffness changes with every loading cycle. D'Alessandro et al. [76] has defined the stiffness ratio by introducing the stiffness ratio function (K_i/K) where K_i indicates the joint secant stiffness during the cycle under study, and K represents the initial stiffness. This function highlights the degradation of joint stiffness over a number of cycles. The K_i is expressed in equation form as:

$$K_i = \frac{|+F_i| + |-F_i|}{|+X_i| + |-X_i|} \quad (2)$$

Here, F_i represents the peak load, and X_i indicates the peak displacement. The plus and minus signs indicate the positive and negative cyclic loading directions, ensuring that the contributions of both side loadings are considered in the stiffness calculation [77]. Figure 13 depicts a gradual decline in the secant stiffness of specimens. This consistent decline reveals the progressive degradation of structural stiffness as the applied cyclic

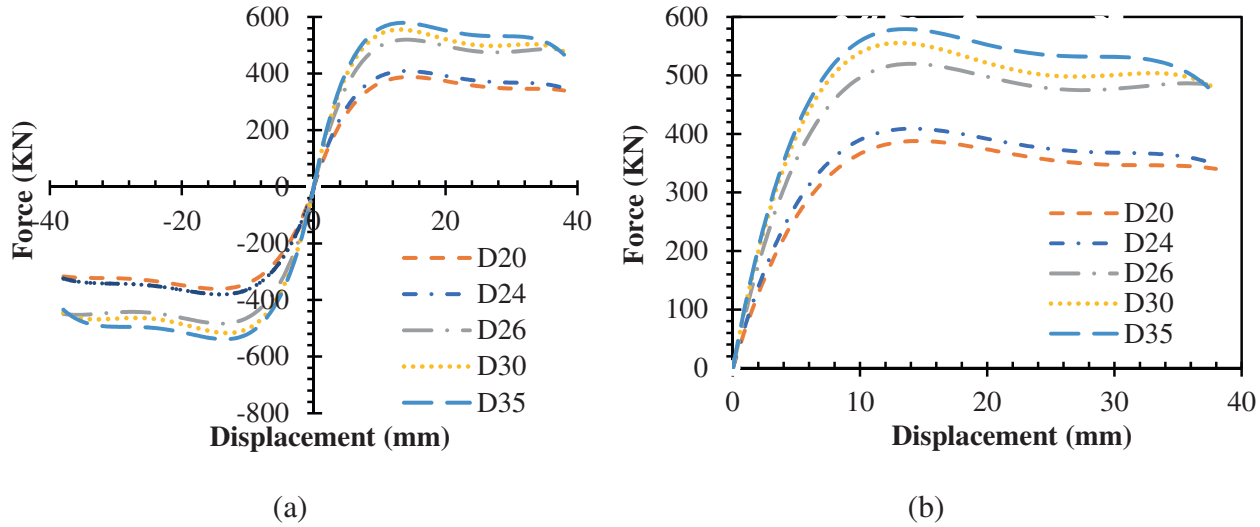

FIGURE 12 | (a) Skeleton curves of tension capacity of IBCJ subjected to cyclic Load and (b) Positive portion of the tension capacity curve.

TABLE 9 | Ductility ratio for different selected bolt sizes.

Bolt	Deformation at yield (mm)	Deformation at failure	μ
D20	3	36	12
D24	3.4	37	10.9
D26	4	39	9.75
D30	6	39	6.5
D35	6.4	39.5	6.2

loading intensifies. Stiffness degradation in steel beam-column joints is primarily attributed to plastic deformations, local buckling, yielding, and the potential loosening or slippage of bolted connections under cyclic loading [78]. When stiffness degradation is minimal, the structure shows greater energy dissipation and ductility, making it better equipped to handle seismic events [79]. In this study, up to a displacement of 20 mm, a rapid loss of secant stiffness is observed across all bolts, followed by a more gradual decline in subsequent loading phases. The D20, D24, and D26 bolts display a similar pattern in stiffness reduction while D30 and D35 bolts exhibit comparatively a slower decline. The resilience shown by larger bolts in maintaining stiffness suggests their capability to mitigate deformations and ensure overall structural integrity under cyclic loading. By carefully monitoring and interpreting these patterns, informed selection of bolts can be followed regarding design modifications and retrofitting measures.

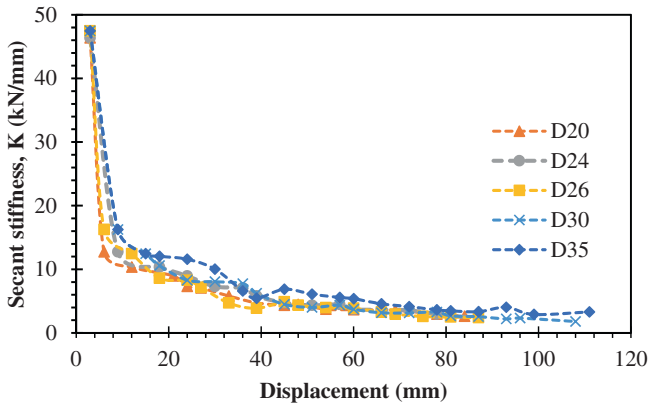

FIGURE 13 | Secant stiffness degradation versus loading displacement curves for each bolt size.

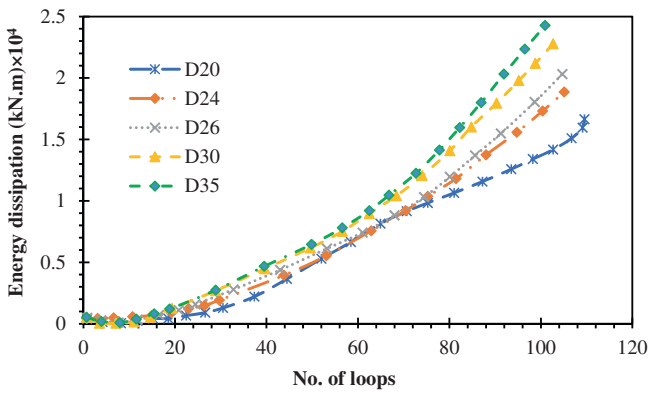

FIGURE 14 | Cumulative energy dissipation across different bolt sizes.

3.7 | Energy Dissipation Capacity

An assessment of energy dissipation is further deemed crucial for performance evaluation of target structure during seismic events. Cumulative dissipated energy, that is, the total amount of energy absorbed or dispersed by a structure subjected to cyclic loading, is evaluated from load–displacement hysteresis graph as the sum of areas under the curves [80]. The wider the area, the higher the dissipated energy, the more capable the structure is to withstand a catastrophic seismic event [81]. Figure 14 represents the energy dissipation trends of bolted connection with different bolt diameters. Larger bolts like D35 and D30, resist higher tensile and shear forces and show greater energy dissipation capacities. However, D26, D24, and D20 bolts indicate a decreasing level of energy dissipation with the decrease in bolt size. The observed pattern

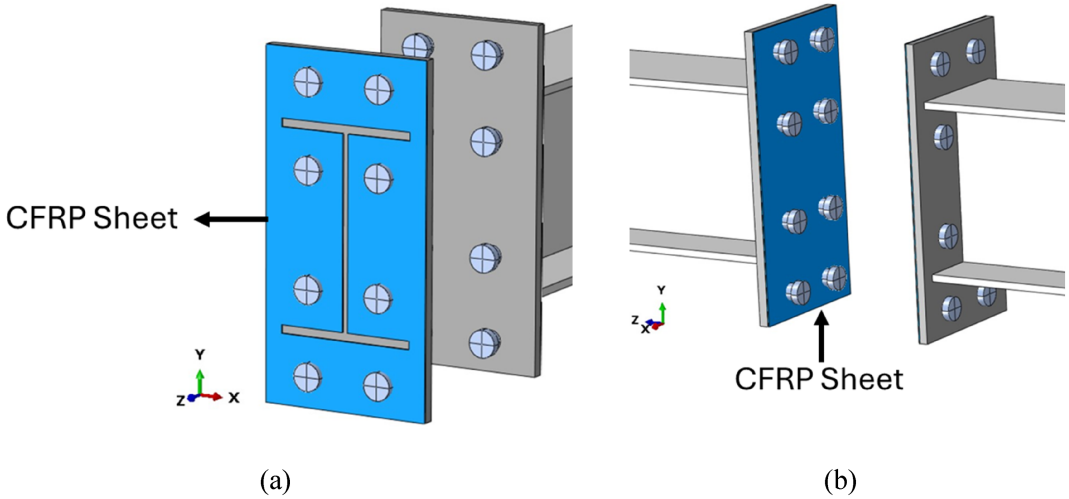

FIGURE 15 | CFRP sheet on the plates: (a) Front side of the plate and (b) Back side of the plate.

indicated the significance of considering bolt diameter in evaluating the seismic energy dissipation performance of the connection.

3.8 | Strengthening of IBCJ With CFRP

The D30 bolt was chosen to further study the effect of CFRP due to its demonstrated superior performance in previous analyses compared to most smaller size bolts. The mentioned bolt exhibited significantly higher ductility (μ) values, which are crucial for maintaining structural integrity under dynamic loading conditions. Additionally, this bolt showed a slower decline in stiffness compared to smaller bolts, indicating their ability to better mitigate deformations and maintain overall structural stability under cyclic loading. Furthermore, it demonstrated better energy dissipation capabilities with minimized deformations at failure under both monotonic and cyclic loading. These characteristics make D30 bolts an optimal choice for assessing the impact of CFRP sheets on the tension capacity enhancement of bolted connections using monotonic loads first. Subsequently, the analysis was carried out on all bolt sizes for both monotonic and cyclic studies after selecting the optimum shape, and location of the CFRP.

3.8.1 | Influence of Location of CFRP Application

From the model validation, it was found that the end plate is more prone to failure in the steel beam-column joint. As a result, it was decided to install CFRP on the extended plate. CFRP was applied to both sides of the plate, first at the front and then at the back. Due to the tie constraint between the plate and the I-beam, CFRP was omitted at the location of the constraint and bolt holes on the front side to ensure proper bonding with the steel plate. For the backside, the CFRP was only omitted where the bolt holes exist, as shown in Figure 15. The tie constraint has been used between the CFRP sheet and the end plate, assuming a perfect bond between them. The analysis revealed that the CFRP on the backside of the plate exhibits greater strength compared to the front side due to the larger excluded area on the front side, as shown in Figure 16.

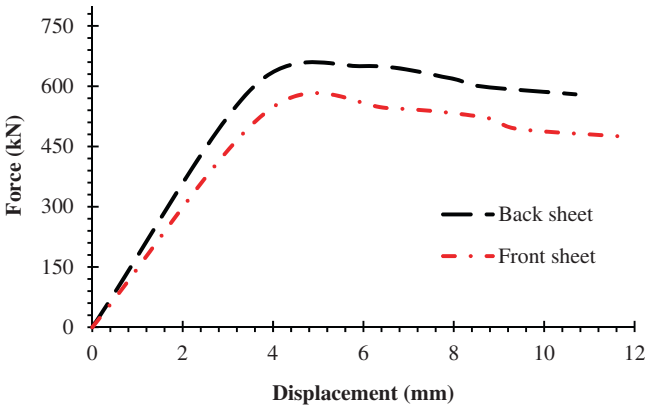

FIGURE 16 | Comparison of the tension capacities of back and front CFRP sheets.

3.8.2 | Effect of Shape of CFRP

Five different shapes of CFRP were tested on the backside of the steel plate, to determine the most optimal shape that provides the best strength, as shown in Figure 17. Also, it was observed from Figure 18 that Case-3 shows the optimal shape to be used as CFRP strengthening technique in steel beam column joint based on its enhanced capabilities of improving the tension capacity of D30 bolt.

3.9 | Influence of CFRP Sheets on Different Bolt Sizes Under Monotonic Loading

After selecting the back side of the plate with case-3 as optimum location for CFRP to be used in steel beam column joint, it was applied on the other bolt sizes as well. Presented in Figure 19, under monotonic loading, application of CFRP resulted in substantial improvement in bolt capacity, ranging from 1.2 to 1.3 times for D30 and D35 bolts, and nearly 1.2 times for D26 and D24 bolts models. For smaller bolts, such as D20, the presence of CFRP marginally contributed to a capacity enhancement of 1.07

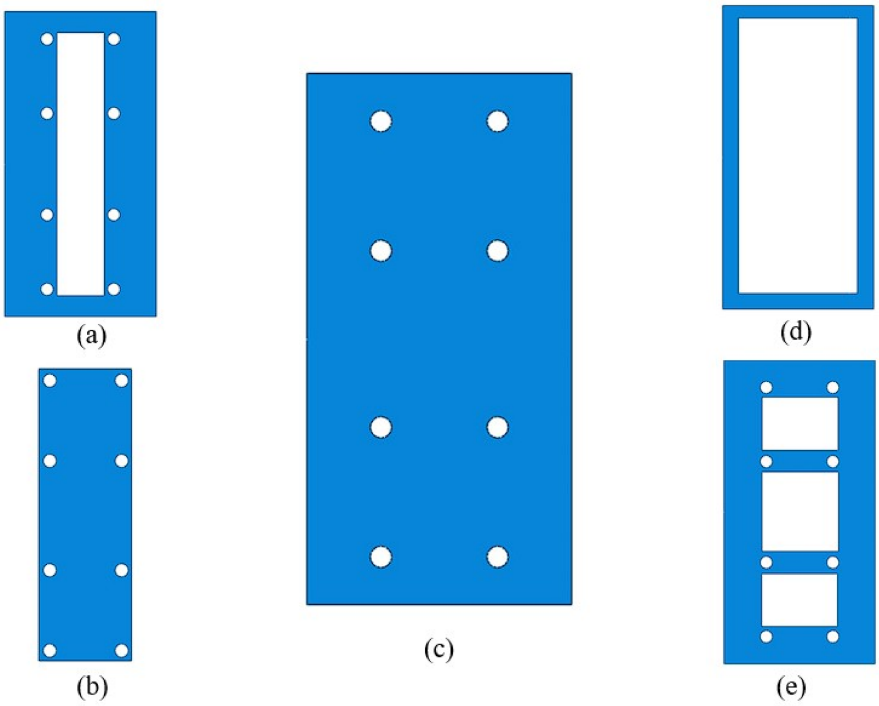

FIGURE 17 | (a) Case-1; (b) Case-2; (c) Case-3; (d) Case-4; and (e) Case-5.

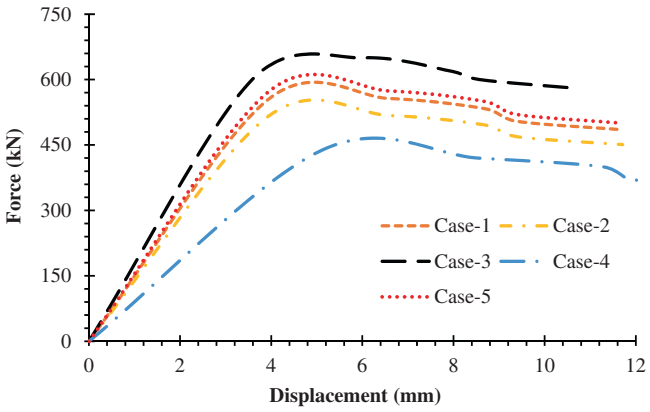

FIGURE 18 | Comparison of the tension capacities of D30 with different shapes of CFRP.

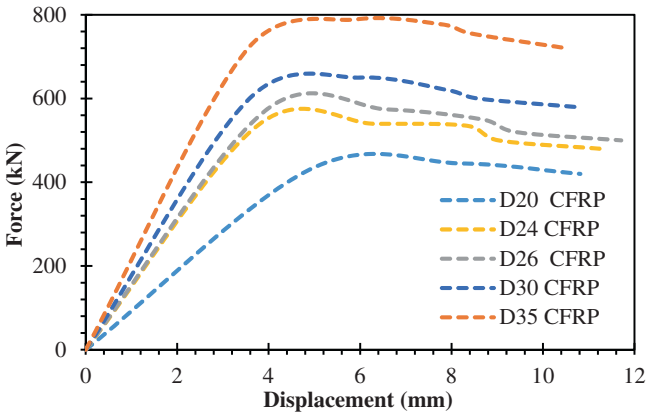

FIGURE 19 | Load (tension) versus displacement curves for various bolt subjected to monotonic loading.

times compared to the models without CFRP. These improvements reflected the effectiveness of CFRP sheets in redistributing and resisting applied loads, reducing the risk of bolt failure, and enhancing structural performance.

3.10 | Influence of CFRP Sheets on Different Bolt Sizes Under Cyclic Loading

To maintain consistency in the implementation of CFRP and enable wider assessment of its impact on the structural behavior under cyclic loading, the same systematic approach has been followed. Figure 20 presents a graphic overview of the tension performance of different bolts with case-3 CFRP application. The results reveal significant enhancement in tension capacity across various bolt sizes. The capacity increases from 1.2 to 1.3 times for D35 and D30 bolt models, and nearly 1.2 times for the smaller bolts like D26 and D24 except D20 where insignificant increase of 1.07 times in strength was observed. The results demonstrated that the installation of CFRP can be an effective solution in improving the resilience of a joint and integrity of overall structure to a seismic event. Moreover, the findings emphasize the significance of CFRP based retrofitting measures, customized application of CFRP sheets for desired performance requirements of structural components of IBCJ.

To summarize the enhancement of the tension capacity of the IBCJ, a comprehensive analysis was conducted systematically, which is outlined here for clarity.

First, the validated FE model with various bolt sizes was analyzed under both monotonic and cyclic loading conditions, with

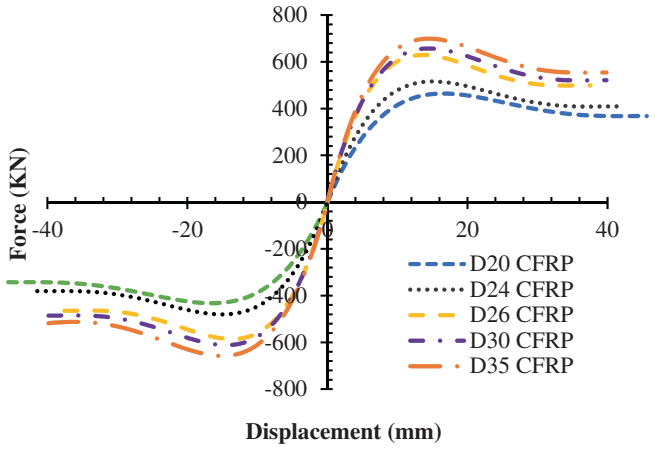

FIGURE 20 | Load (tension) versus displacement curves for various bolts subjected to cyclic loading.

the tension capacity results presented in Figures 10 and 11. The model with a D30 bolt was identified as the most suitable IBCJ model for CFRP application on both sides of the end plate. The back side of the end plate was determined to be the optimal location for CFRP installation, significantly improving tension capacity, as shown in Figure 15.

Subsequently, the shape of the CFRP sheet was optimized across different cases to balance performance and cost. Case-3 emerged as the most effective strengthening technique for enhancing the IBCJ's tension capacity, as demonstrated in Figure 17. Finally, Case-3 was applied to a range of bolt sizes, showing a 1.2 to 1.3 times improvement in the tension capacity of the IBCJ, as illustrated in Figures 18 and 19.

4 | Conclusions

This study employed a FEM and analysis approach to examine the behavior of steel IBCJ under both monotonic and cyclic loading. Initially, the experimental beam-column joint was modeled in FEM, followed by result validation, tension capacity analysis, and assessment of ductility ratio, secant stiffness, and energy dissipation capacity for D20, D24, D26, D30, and D35 bolts. Subsequently, CFRP sheets were modeled and applied to the back side of the endplates of the steel IBCJ to assess their impact on the tension capacity of the bolted connection. The key findings of the study are as follows:

- Larger bolts, such as D30 and D35, exhibited higher ultimate capacities and minimized deformations at failure under both monotonic and cyclic loading.
- A significantly larger ductility ratio of about 6 and higher energy dissipation capacity for D30 and D35 bolts indicated significant joint resilience. Therefore, prioritizing these bolts is recommended for enhanced ductile behavior and superior energy dissipation capacity in seismic zones.
- Applying CFRP sheet to the back side of end plates with minimum excluded area (Case-3) proved to be a promising solution for improving performance of steel beam-column joints and bolt load capacities.
- The CFRP sheet on the backside has potential to increase the tension capacity of bolts by approximately 1.2 to 1.3 times, making it a feasible retrofitting strategy that could enhance overall structural performance.
- Smaller bolts have the potential to achieve superior joint capacity when complemented with CFRP, showcasing the effectiveness of this reinforcement method across a range of bolt sizes.

Based on the analysis and results, this study recommends prioritizing the use of larger bolt sizes, such as D30 and D35, to enhance the seismic performance of structures under both monotonic and cyclic loadings. In seismic zones, selecting bolts with higher ductility ratios, secant stiffness, and cumulative dissipated energy will be crucial for improving joint resilience. Smaller bolt sizes could also be considered if the endplate of a joint is strengthened with CFRP sheets, as this can achieve superior joint capacity. Detailed examination of CFRP sheets, including their thickness and feasibility for strengthening and retrofitting various structural elements, is recommended. Additionally, experimental testing is recommended to ensure the practicality of numerical outcomes for CFRP application at beam-column joints under both monotonic and cyclic loadings.

Author Contributions

Fayiz Amin: conceptualization, methodology, validation, formal analysis, writing – original draft. **Hafiz Ahmed Waqas:** conceptualization, formal analysis, supervision. **Ijaz Ali:** methodology, formal analysis. **Muhammad Waseem:** writing – review and editing, data curation. **Muhammad Asif:** writing – original draft, formal analysis, data curation, methodology. **Khan Abdul Majid:** validation, software, conceptualization. **Megersa Kebede Leta:** supervision, writing – review and editing, data curation, visualization.

Conflicts of Interest

The authors declare no conflicts of interest.

Data Availability Statement

The data that support the findings of this study are available from the corresponding author upon reasonable request.

References

1. X. Cao, X. Li, Y. Zhu, and Z. Zhang, "A Comparative Study of Environmental Performance Between Prefabricated and Traditional Residential Buildings in China," *Journal of Cleaner Production* 109 (2015): 131–143, https://doi.org/10.1016/j.jclepro.2015.04.120.

2. N. Krishnamurthy, "A Fresh Look at Bolted End-Plate Behavior and Design," *Engineering Journal* 15, no. 2 (1978): 39–49, https://doi.org/10.62913/engj.v15i2.311.

3. Y.-S. Yu and X.-Y. Liu, "Finite Element Analyses on Energy Dissipation Capacity of Upper Flange Welded-Lower Flange Bolted Beam-Column Connection With Slotted Holes," *Journal of Asian Architecture and Building Engineering* 19, no. 4 (2020): 315–326, https://doi.org/10.1080/13467581.2020.1749639.

4. J. Hong, G. Q. Shen, Z. Li, B. Zhang, and W. Zhang, "Barriers to Promoting Prefabricated Construction in China: A Cost–Benefit Analysis," *Journal of Cleaner Production* 172 (2018): 649–660, https://doi.org/10.1016/j.jclepro.2017.10.171.

5. X. C. Liu, S. H. Pu, A. L. Zhang, et al., "Static and Seismic Experiment for Bolted-Welded Joint in Modularized Prefabricated Steel Structure," *Journal of Constructional Steel Research* 115 (2015): 417–433, https://doi.org/10.1016/j.jcsr.2015.08.036.

6. W. S. Ansari, *A Statistical Review of Offsite Construction Techniques in Pakistan* (Saarbrucken, Germany: LAP Lambert Academic Publishing, 2017).

7. D. K. Miller, "Lessons Learned From the Northridge Earthquake," *Engineering Structures* 20, no. 4–6 (1998): 249–260, https://doi.org/10.1016/S0141-0296(97)00031-X.

8. S. A. Mahin, "Lessons From Damage to Steel Buildings During the Northridge Earthquake," *Engineering Structures* 20, no. 4–6 (1998): 261–270, https://doi.org/10.1016/S0141-0296(97)00032-1.

9. T. Kim and J. Kim, "Collapse Analysis of Steel Moment Frames With Various Seismic Connections," *Journal of Constructional Steel Research* 65, no. 6 (2009): 1316–1322, https://doi.org/10.1016/j.jcsr.2008.11.006.

10. M. Ilyas, A. Ahmad, A. Riaz, et al., "Review of Modeling Techniques for Analysis and Assessment of RC Beam–Column Joints Subjected to Seismic Loads," *Materials* 15, no. 21 (2022): 7448, https://doi.org/10.3390/MA15217448.

11. H. A. Waqas, M. Sahil, M. M. Khan, A. W. Anwar, M. U. Shah, and M. Usman, "Optimizing Reinforcement Strategies for Robust Beam-Column Joints in Seismic-Resistant Structures," *Arabian Journal for Science and Engineering* 49, no. 4 (2024): 6107–6124, https://doi.org/10.1007/S13369-023-08591-1/METRICS.

12. F. Amin, H. A. Waqas, M. Alam, et al., "Strengthening of Reinforced Concrete Deep Beams With Large Openings Using Metal Plates," *Emirati Journal of Civil Engineering and Applications* 1, no. 1 (2023): 31–44, https://doi.org/10.54878/0NGK5130.

13. Y. I. Maggi, R. M. Gonçalves, R. T. Leon, and L. F. L. Ribeiro, "Parametric Analysis of Steel Bolted End Plate Connections Using Finite Element Modeling," *Journal of Constructional Steel Research* 61, no. 5 (2005): 689–708, https://doi.org/10.1016/j.jcsr.2004.12.001.

14. L. Leigh, "Analysis and Comparison of Connections in Steel Structures," (PhD diss., Massachusetts Institute of Technology, 2006).

15. A. N. T. Ihaddoudène, M. Saidani, and M. Chemrouk, "Mechanical Model for the Analysis of Steel Frames With Semi Rigid Joints," *Journal of Constructional Steel Research* 65, no. 3 (2009): 631–640, https://doi.org/10.1016/j.jcsr.2008.08.010.

16. L. R. O. de Lima, S. A. L. de Andrade, P. C. G. d. S. Vellasco, and L. S. d. Silva, "Experimental and Mechanical Model for Predicting the Behaviour of Minor Axis Beam-to-Column Semi-Rigid Joints," *International Journal of Mechanical Sciences* 44, no. 6 (2002): 1047–1065, https://doi.org/10.1016/S0020-7403(02)00013-9.

17. M. Sahil, A. Bahrami, H. A. Waqas, et al., "Seismic Performance Evaluation of Exterior Reinforced Concrete Beam-Column Connections Retrofitted With Economical Perforated Steel Haunches," *Results in Engineering* 22 (2024): 102179, https://doi.org/10.1016/J.RINENG.2024.102179.

18. L. Luo, J. Qin, D. Zhao, and Z. Wu, "Seismic Behavior of Extended End-Plate Connections Subjected to Cyclic Loading on the Top-Side of the Column," *Materials* 13, no. 17 (2020): 3724, https://doi.org/10.3390/ma13173724.

19. K. F. Chung and K. H. Ip, "Finite Element Investigation on the Structural Behaviour of Cold-Formed Steel Bolted Connections," *Engineering Structures* 23, no. 9 (2001): 1115–1125, https://doi.org/10.1016/S0141-0296(01)00006-2.

20. E. Mashaly, M. El-Heweity, H. Abou-Elfath, and M. Osman, "Finite Element Analysis of Beam-to-Column Joints in Steel Frames Under Cyclic Loading," *Alexandria Engineering Journal* 50, no. 1 (2011): 91–104, https://doi.org/10.1016/j.aej.2011.01.012.

21. H. B. Blum and K. J. Rasmussen, "Finite Element Analysis of Cold-Formed Steel Connections," *International Journal of Engineering (IJE)* 5, no. 2 (2011): 55–61.

22. X. C. Liu, S. H. Pu, A. L. Zhang, and X. X. Zhan, "Performance Analysis and Design of Bolted Connections in Modularized Prefabricated Steel Structures," *Journal of Constructional Steel Research* 133 (2017): 360–373, https://doi.org/10.1016/j.jcsr.2017.02.025.

23. R. E. S. Ismail, A. S. Fahmy, A. M. Khalifa, and Y. M. Mohamed, "Numerical Study on Ultimate Behaviour of Bolted End-Plate Steel Connections," *Latin American Journal of Solids and Structures* 13, no. 1 (2016): 1–22, https://doi.org/10.1590/1679-78251579.

24. A. K. Dessouki, A. H. Youssef, and M. M. Ibrahim, "Behavior of I-Beam Bolted Extended End-Plate Moment Connections," *Ain Shams Engineering Journal* 4, no. 4 (2013): 685–699, https://doi.org/10.1016/j.asej.2013.03.004.

25. C.-C. Chen, S.-W. Chen, M.-D. Chung, and M.-C. Lin, "Cyclic Behaviour of Unreinforced and Rib-Reinforced Moment Connections," *Journal of Constructional Steel Research* 61, no. 1 (2005): 1–21, https://doi.org/10.1016/j.jcsr.2004.06.005.

26. J. Fan, J. Zhao, Q. Zhu, Z. Ni, and J. Liu, "Seismic Behavior and Analytical Model for a Fully Bolted Joint Between CFDST Columns and Steel Beams," *Structure* 42 (2022): 515–530, https://doi.org/10.1016/j.istruc.2022.06.033.

27. A. ElSabbagh, T. Sharaf, S. Nagy, and M. ElGhandour, "Behavior of Extended End-Plate Bolted Connections Subjected to Monotonic and Cyclic Loads," *Engineering Structures* 190 (2019): 142–159, https://doi.org/10.1016/j.engstruct.2019.04.016.

28. I. A. Bukhari, R. L. Vollum, S. Ahmad, and J. Sagaseta, "Shear Strengthening of Reinforced Concrete Beams With CFRP," *Magazine of Concrete Research* 62, no. 1 (2010): 65–77, https://doi.org/10.1680/MACR.2008.62.1.65.

29. D. H. Vo, V. H. Do, Q. V. Tran, M. H. Nguyen, and T. L. Hoang, "Reliability Analysis of Steel Bridge Girders Strengthened With CFRP Considering the Debonding of Adhesive Layer," *Designs* 6, no. 6 (2022): 126, https://doi.org/10.3390/DESIGNS6060126.

30. R. Sen, L. Liby, and G. Mullins, "Strengthening Steel Bridge Sections Using CFRP Laminates," *Composites Part B: Engineering* 32, no. 4 (2001): 309–322, https://doi.org/10.1016/S1359-8368(01)00006-3.

31. H. A. Waqas, A. Bahrami, F. Amin, M. Sahil, and M. Saud Khan, "Numerical Modeling and Performance Evaluation of Carbon Fiber-Reinforced Polymer-Strengthened Concrete Culverts Against Water-Induced Corrosion," *Infrastructures* 9, no. 5 (2024): 82, https://doi.org/10.3390/INFRASTRUCTURES9050082.

32. T. Miller, M. Chajes, D. Mertz, and J. Hastings, "Strengthening of a Steel Bridge Girder Using CFRP Plates," *Journal of Bridge Engineering* 6 (2001): 514–522, https://doi.org/10.1061/(ASCE)1084-0702(2001)6:6(514).

33. X. Liu and A. Nanni, *Rehabilitation of Steel Bridge Members With FRP Composite Materials* (Amsterdam, Netherlands: University of Missouri-Rolla, 2001).

34. J. Cadei, T. Stratford, L. Hollaway, and W. Duckett, *Strengthening Metallic Structures Using Externally Bonded Fibre-Reinforced Polymers* (Basel, Switzerland: Ciria, 2004).

35. E. Sayed-Ahmed, "Strengthening of Thin-Walled Steel I-Section Beams Using CFRP Strips," *Advanced Composite Materials in Bridges and Structures, Conference Paper, 4th International Conference on Advanced Composite Materials in Bridges and Structures* (*ACMBS IV*) (Calgary, Alberta, Canada, 2004).

36. E. Sayed-Ahmed, "Numerical Investigation Into Strengthening Steel I-Section Beams Using CFRP Strips," in *Structures Congress 2006: Structural Engineering and Public Safety*, 1–8 (2006), https://doi.org/10.1061/40889(201)68.

37. M. A. Ghareeb, M. A. Khedr, and E. Y. Sayed-Ahmed, "CFRP Strengthening of Steel I-Beam Against Local Web Buckling: A Numerical Analysis," in *Research and Applications in Structural Engineering, Mechanics and Computation* (London, UK: CRC Press, 2013), 897–898, https://doi.org/10.1201/b15963-436.

38. M. Shekarchi and A. Khaloo, "Shear and Flexural Strengthening of Steel Beams With Thick Carbon Fiber Reinforced Polymer Laminate," *Journal of Rehabilitation in Civil Engineering* 9, no. 4 (2021): 148–170, https://doi.org/10.22075/JRCE.2021.22339.1473.

39. P. Colombi and C. Poggi, "Strengthening of Tensile Steel Members and Bolted Joints Using Adhesively Bonded CFRP Plates," *Construction and Building Materials* 20, no. 1–2 (2006): 22–33, https://doi.org/10.1016/j.conbuildmat.2005.06.042.

40. Y. O. Özkilic, "Investigation of the Effects of Bolt Diameter and End-Plate Thickness on the Capacity and Failure Modes of End-Plated Beam-to-Column Connections," *Research on Engineering Structures and Materials* 7, no. 3 (2021): 445–463, https://doi.org/10.17515/resm2021.275st0315.

41. J. T. Mottram and Y. Zheng, "Further Tests of Beam-to-Column Connections for Pultruded Frames: Flange-Cleated," *Journal of Composites for Construction* 3, no. 3 (1999): 108–116, https://doi.org/10.1061/(ASCE)1090-0268(1999)3:3(108).

42. J. T. Mottram and Y. Zheng, "State-of-the-Art Review on the Design of Beam-to-Column Connections for Pultruded Frames," *Composite Structures* 35, no. 4 (1996): 387–401, https://doi.org/10.1016/S0263-8223(96)00052-9.

43. B. Zafari and J. T. Mottram, "Characterization by Full-Size Testing of Pultruded Frame Joints for the Startlink House," *Journal of Composites for Construction* 19, no. 1 (2015): 04014033, https://doi.org/10.1061/(ASCE)CC.1943-5614.0000488.

44. B. Zafari and J. T. Mottram, "Effect of Hot-Wet Aging on the Pin-Bearing Strength of a Pultruded Material With Polyester Matrix," *Journal of Composites for Construction* 16, no. 3 (2012): 340–352, https://doi.org/10.1061/(ASCE)CC.1943-5614.0000258.

45. J. Qureshi and J. T. Mottram, "Moment-Rotation Response of Nominally Pinned Beam-to-Column Joints for Frames of Pultruded Fibre Reinforced Polymer," *Construction and Building Materials* 77 (2015): 396–403, https://doi.org/10.1016/j.conbuildmat.2014.12.057.

46. J. Qureshi and J. T. Mottram, "Behaviour of Pultruded Beam-to-Column Joints Using Steel Web Cleats," *Thin-Walled Structures* 73 (2013): 48–56, https://doi.org/10.1016/j.tws.2013.06.019.

47. J. Qureshi and J. T. Mottram, "Response of Beam-to-Column Web Cleated Joints for FRP Pultruded Members," *Journal of Composites for Construction* 18, no. 2 (2014): 04013039, https://doi.org/10.1061/(ASCE)CC.1943-5614.0000392.

48. J. Qureshi, Y. Nadir, and S. K. John, "Bolted and Bonded FRP Beam-Column Joints With Semi-Rigid End Conditions," *Composite Structures* 247 (2020): 112500, https://doi.org/10.1016/j.compstruct.2020.112500.

49. S. J. Smith, I. D. Parsons, and K. D. Hjelmstad, "Experimental Comparisons of Connections for GFRP Pultruded Frames," *Journal of Composites for Construction* 3, no. 1 (1999): 20–26, https://doi.org/10.1061/(ASCE)1090-0268(1999)3:1(20).

50. J. E. Carrion, J. M. LaFave, and K. D. Hjelmstad, "Experimental Behavior of Monolithic Composite Cuff Connections for Fiber Reinforced Plastic Box Sections," *Composite Structures* 67, no. 3 (2005): 333–345, https://doi.org/10.1016/j.compstruct.2004.01.015.

51. D. Martins, M. Proença, J. Almeida Gonilha, M. Figueiredo Sá, J. Ramôa Correia, and N. Silvestre, "Experimental and Numerical Analysis of GFRP Frame Structures. Part 1: Cyclic Behaviour at the Connection Level," *Composite Structures* 220 (2019): 304–317, https://doi.org/10.1016/j.compstruct.2019.03.097.

52. D. Martins, M. Figueiredo Sá, J. Almeida Gonilha, J. Ramôa Correia, N. Silvestre, and J. Gomes Ferreira, "Experimental and Numerical Analysis of GFRP Frame Structures. Part 2: Monotonic and Cyclic Sway Behaviour of Plane Frames," *Composite Structures* 220 (2019): 194–208, https://doi.org/10.1016/j.compstruct.2019.03.098.

53. D. Martins, J. Gonilha, J. R. Correia, and N. Silvestre, "Exterior Beam-to-Column Bolted Connections Between GFRP I-Shaped Pultruded Profiles Using Stainless Steel Cleats. Part 1: Experimental Study," *Thin-Walled Structures* 163 (2021): 107719, https://doi.org/10.1016/j.tws.2021.107719.

54. M. Bruneau and D. Walker, "Cyclic Testing of Pultruded Fiber-Reinforced Plastic Beam-Column Rigid Connection," *Journal of Structural Engineering* 120, no. 9 (1994): 2637–2652, https://doi.org/10.1061/(ASCE)0733-9445(1994)120:9(2637).

55. C. Qiu, Y. Bai, Z. Cai, and Z. Zhang, "Cyclic Performance of Splice Connections for Hollow Section Fibre Reinforced Polymer Members," *Composite Structures* 243 (2020): 112222, https://doi.org/10.1016/j.compstruct.2020.112222.

56. M. Delzendeh Moghadam, A. Fathi, and O. Chaallal, "Retrofitting of Steel Structures With CFRP: Literature Review and Research Needs," *Applied Sciences* 14, no. 13 (2024): 5958, https://doi.org/10.3390/app14135958.

57. N. B. Accord and C. J. Earls, "Use of Fiber-Reinforced Polymer Composite Elements to Enhance Structural Steel Member Ductility," *Journal of Composites for Construction* 10, no. 4 (2006): 337–344, https://doi.org/10.1061/(ASCE)1090-0268(2006)10:4(337).

58. W. F. Ragheb, "Elastic Local Buckling of Steel I-Sections Strengthened With Bonded FRP Strips," *Journal of Constructional Steel Research* 107 (2015): 81–93, https://doi.org/10.1016/j.jcsr.2015.01.009.

59. W. F. Ragheb, "Inelastic Local Buckling and Rotation Capacity of Steel I-Beams Strengthened With Bonded FRP Sheets," *Journal of Composites for Construction* 21, no. 1 (2017): 04016058, https://doi.org/10.1061/(ASCE)CC.1943-5614.0000716.

60. H. Liu, R. Al-Mahaidi, and X.-L. Zhao, "Experimental Study of Fatigue Crack Growth Behaviour in Adhesively Reinforced Steel Structures," *Composite Structures* 90, no. 1 (2009): 12–20, https://doi.org/10.1016/j.compstruct.2009.02.016.

61. E. Mashaly, M. El-Heweity, H. Abou-Elfath, and M. Osman, "Behavior of Four-Bolt Extended End-Plate Connection Subjected to Lateral Loading," *Alexandria Engineering Journal* 50, no. 1 (2011): 79–90, https://doi.org/10.1016/j.aej.2011.01.011.

62. M. PRC, *Chinese Standard. GB 50017–2017. Code for Design of Steel Structure* (Beijing, China: China Building Industry Press, 2017).

63. Y. B. Sudhir Sastry, P. R. Budarapu, Y. Krishna, and S. Devaraj, "Studies on Ballistic Impact of the Composite Panels," *Theoretical and Applied Fracture Mechanics* 72, no. 1 (2014): 2–12, https://doi.org/10.1016/J.TAFMEC.2014.07.010.

64. British Standard, *Metallic Materials—Tensile Testing, GB/T228.1—2010* (Amsterdam, Netherlands: National Standard of People's Republic of China, 2010).

65. J. Zhang and X. Zhang, "Simulating Low-Velocity Impact Induced Delamination in Composites by a Quasi-Static Load Model With Surface-Based Cohesive Contact," *Composite Structures* 125 (2015): 51–57, https://doi.org/10.1016/J.COMPSTRUCT.2015.01.050.

66. Z. Hashin, "Failure Criteria for Unidirectional Fiber Composites," *Journal of Applied Mechanics* 47, no. 2 (1980): 329–334, https://doi.org/10.1115/1.3153664.

67. D. K. Shin, H. C. Kim, and J. J. Lee, "Numerical Analysis of the Damage Behavior of an Aluminum/CFRP Hybrid Beam Under Three Point Bending," *Composites Part B: Engineering* 56 (2014): 397–407, https://doi.org/10.1016/J.COMPOSITESB.2013.08.030.

68. H. Zhao, G. Shi, X. Chen, and T. Xiao, "Numerical Simulation and Mechanical Model of Steel Beam-to-Column Joints Retrofitted by Haunches," *Journal of Constructional Steel Research* 185 (2021): 106858, https://doi.org/10.1016/j.jcsr.2021.106858.

69. Y. Rahmi, A. Saputra, and S. Siswosukarto, "Numerical Modelling of Interior RC Beam-Column Joints for Non-Engineered Buildings Strengthened Using Steel Plates," in *MATEC Web of Conferences* (London, UK: EDP Sciences, 2017), https://doi.org/10.1051/matecconf/201713802007.

70. P. W. Clark, *Protocol for Fabrication, Inspection, Testing and Documentation of Beam-Colum Connection Tests and Other Experimental Specimens* (Amsterdam, Netherlands: SAC Joint Venture, 2002).

71. P. Paudel, S. Dulal, M. Bhandari, and A. Kumar Tomar, "Study on Pre-Fabricated Modular and Steel Structures," 2016, http://www.internationaljournalssrg.org/.

72. F. Amin, A. Bahrami, H. A. Waqas, et al., "Influence of Arch Action on Load-Carrying Capacity of Double-Sized Industrial Precast Slabs: A Combined Numerical and Experimental Study," *Results in Materials* 23 (2024): 100575, https://doi.org/10.1016/j.rinma.2024.100575.

73. M. Rakhshanimehr, M. R. Esfahani, M. R. Kianoush, B. A. Mohammadzadeh, and S. R. Mousavi, "Flexural Ductility of Reinforced Concrete Beams With Lap-Spliced Bars," *Canadian Journal of Civil Engineering* 41, no. 7 (2014): 594–604, https://doi.org/10.1139/CJCE-2013-0074.

74. H. Dabiri, K. Rahimzadeh, and A. Kheyroddin, "A Comparison of Machine Learning- and Regression-Based Models for Predicting Ductility Ratio of RC Beam-Column Joints," *Structure* 37 (2022): 69–81, https://doi.org/10.1016/j.istruc.2021.12.083.

75. A. K. Chopra, "Dynamics of Structures," 4th ed. Prentice-Hall International Series in Civil Engineering and Engineering Mechanics, 2011, accessed May 06, 2024, https://books.google.com/books/about/Dynamics_of_Structures.html?hl=tr&id=3cctkgEACAAJ.

76. E. D'Alessandro, G. Brando, and G. De Matteis, "Design Charts for End-Plate Beam-to-Column Steel Joints," *Proceedings of the Institution of Civil Engineers: Structures and Buildings* 171, no. 6 (2018): 444–462, https://doi.org/10.1680/jstbu.16.00203.

77. X. Ni, S. Cao, Y. Li, and S. Liang, "Stiffness Degradation of Shear Walls Under Cyclic Loading: Experimental Study and Modelling," *Bulletin of Earthquake Engineering* 17, no. 9 (2019): 5183–5216, https://doi.org/10.1007/s10518-019-00682-5.

78. W. B. Banu, K. P. Jaya, and R. Vidjeapriya, "Seismic Behaviour of Exterior Beam-Column Joint Using Steel Fibre-Reinforced Concrete Under Reverse Cyclic Loading," *Arabian Journal for Science and Engineering* 48, no. 4 (2023): 4635–4655, https://doi.org/10.1007/s13369-022-07139-z.

79. T. Wang, M. Noori, W. A. Altabey, et al., "From Model-Driven to Data-Driven: A Review of Hysteresis Modeling in Structural and Mechanical Systems," *Mechanical Systems and Signal Processing* 204 (2023): 110785, https://doi.org/10.1016/j.ymssp.2023.110785.

80. M. J. N. Priestley and G. A. MacRae, "Seismic Tests of Precast Beam-to-Column Joint Subassemblages With Unbonded Tendons," *PCI Journal* 41, no. 1 (1996): 64–80, https://doi.org/10.15554/PCIJ.01011996.64.81.

81. A. Mokha, M. C. Constantinou, A. M. Reinhorn, and V. A. Zayas, "Experimental Study of Friction-Pendulum Isolation System," *Journal of Structural Engineering* 117, no. 4 (1991): 1201–1217, https://doi.org/10.1061/(ASCE)0733-9445(1991)117:4(1201).